Accepted manuscript doi:
10.1680/jgeot.17.p.053

Accepted manuscript doi: 10.1680/jgeot.17.p.053

Submitted: 26 February 2017

Published online in 'accepted manuscript' format: 20 July 2018

Manuscript title: Experimental microscopic investigation of the cyclic swelling and shrinkage of a natural hard clay

Authors: Diansen Yang*,†, Weizhong Chen*,†, Linlin Wang‡, Liufeng Chen§ and Wei Wang*,†

Affiliations: *State Key Laboratory of Geomechanics and Geotechnical Engineering, IRSM, Chinese Academy of Science, Wuhan 430071, China; †University of Chinese Academy of Sciences, Beijing 100049, China; ‡College of Petroleum Engineering, China University of Petroleum (Beijing), Beijing 102249, China; §School of Civil and Architectural Engineering, Wuhan University, Wuhan 430072, China

Corresponding author: Linlin Wang, College of Petroleum Engineering, China University of Petroleum (Beijing), Beijing 102249, China.

E-mail: blaisewang@msn.com

ABSTRACT

In this paper, we present a microscopic experimental investigation of the swelling-shrinkage behaviour of a hard clay subjected to wetting and drying (W-D) cycles. Three W-D cycles with a range of relative humidity from 20% to 98% were performed on the hard clay sample through varying the temperature and the vapour pressure in an environmental scanning electron microscope (ESEM). The obtained ESEM images of the material at different hydric stages were analysed using digital image correlation method, and full-field strains at the micrometer scale, were quantified. The results show that the deformation of the material when subjected to W-D cycles is significantly heterogeneous and it is closely related to its microstructure. The different contributions of clay particles and of inclusions to swelling and shrinkage of the hard clay are revealed: the clay minerals swell, which is however constrained by the no-swelling inclusions; the interaction between the different phases is significant. A residual swelling is found at the end of the first W-D cycle. The residual swelling continues to accumulate during the second cycle but becomes stable for the third cycle. Further microstructural analysis shows that the irreversible swelling is mainly attributed to the appearance and propagation of microcracks accompanied with a limited unrecoverable deformation of the clay minerals.

KEYWORDS: wetting and drying; cyclic swelling and shrinkage; microstructure; hard clay; microcracks

Accepted manuscript doi:
10.1680/jgeot.17.p.053

1. Introduction

Due to seasonal change of weather conditions (e.g. temperature, humidity, wind, rainfall), clayey materials are often subjected to cyclic wetting and drying (W-D). During these W-D cycles, the materials swell and shrink (Mitchell and Soga, 2005). The hydric deformation (i.e. swelling and shrinkage) and the induced deterioration in the hydromechanical properties during W-D cycles may induce natural hazard (e.g. landslides, desiccation cracking) and severe damage to man-made structures (e.g., buildings, tunnels) (Meisina, 2004; Tsang et al., 2005; Yang et al., 2012, 2013; Torres-Suarez et al., 2014; Eid et al., 2015). Therefore, swelling/shrinkage is a major concern in many domains such as construction of structures in clayey materials.

In the past decades, a significant number of studies (Osipov et al., 1987; Alonso et al., 2005; Sivakumar et al., 2006; Laribi et al., 2008; Delage et al., 2014) have been conducted to investigate the deformation and the induced changes in hydromechanical properties of clayey materials during W-D cycles. The hydromechanical properties (e.g. stiffness, strength, and permeability) vary during wetting (Aksua et al., 2015, Wang et al., 2015). Some researchers (e.g. Wheeler et al., 2003; Alonso et al., 2005) studied the cyclic W-D behaviour of the clayey soils and found the irreversible shrinkage occurs during successive cycles of W-D until finally a reversible elastic response occurs. Wang et al. (2014a) studied free swelling and shrinkage of Collovo-Oxfordian argillaceous rock and found cracking emerges during the W-D cycle. Most of the existing studies employ oedometer tests and triaxial tests to quantify swelling and shrinkage, and we call these studies as macroscopic studies. A few investigations focus on the swelling and shrinkage mechanism of clay minerals using different microscopy measurements (e.g. X-ray, mercury intrusion porosimetry, scanning electron microscopy) (Viola et al., 2005; Koliji et al., 2006; Amorim et al., 2007; Romero and Simms, 2008; Burton et al., 2015; Ma et al., 2015). Through microscopic investigation, it is acknowledged that swelling of pure clay minerals occurs via two different regimes: crystalline and osmotic swelling. Crystalline swelling is driven by adsorption of water molecules in interlayer region, while osmotic swelling is related to the difference in the solute concentration of clay-water system and involves inter-particle separations (Delville and Laszlo, 1990; Mitchell and Soga, 2005; Anderson et al., 2010). However, swelling and shrinkage are still not well understood for natural clayey material subjected to W-D cycles, because the material has complex microstructures in comparison with pure clays.

Recently, environmental scanning electron microscope (ESEM) is used to study swelling and shrinkage of clayey material under controlled humidity (Viola et al., 2005; Montes-H et al., 2003). ESEM is also combined with image processing such as digital image correlation technique (DIC) by several researchers (Wang et al., 2013, 2014a, 2015) to determine the swelling of clayey material at the micrometric scale. Compared with qualitative observation conventionally used with ESEM, the combination of ESEM and DIC can provide quantitative investigation of the microstructure change of the tested material when subjected to W-D.

In this paper, we will perform cyclic W-D tests on a hard clay sample in ESEM and quantitatively explore the microstructure change of the material through analysing the ESEM images by DIC. The used experimental method will be presented in the second section, and the studied material and the experimental process will be presented in the third part, followed with the results and discussions on the swelling and shrinkage of the hard clay subjected to three W-D cycles.

2. Experimental method

Wetting and drying in ESEM

In this study, wetting and drying tests are carried out in an environment scanning electron microscope (ESEM) equipped with a Peltier module that can control the temperature of the sample deposing on it. Based on the definition, the relative humidity (RH) can be adjusted by changing water vapour pressure and temperature. During this test, the temperature is kept at 2°C, and the gas pressure is varied to obtain target RH. The choice of low temperature is because, for a given RH, low temperature corresponds to low water vapour pressure so that the images are less degraded. This is vital for the accuracy of strain measurement using DIC. When the sample reaches the hydric equilibrium, a zone of interest will be recorded in the backscattered electron model (BSE). BSE image contains information about chemical composition and exhibits a contrast of phase density, which is appropriate for identification of the microstructure of the tested material. More information about this wetting test method can be found in Wang et al., (2013).

Full-field strains determined by DIC

The obtained high-resolution images of the material at different hydric states are analyzed using digital image correlation (DIC) technique. DIC, first proposed in the 1980s and has made enormous development in the past decades, has been widely used in many disciplines such as solid mechanics and materials sciences (Sutton et al., 2009; Bornert et al., 2011). Once the correlation is determined, the discrete displacement field is evaluated, and the local strain will be then quantified by averaging the infinitesimal gradient over a certain zone (Allais et al., 1994). A DIC program was used to determine the in-plane components of local strains (ε_{xx}, ε_{yy}, ε_{xy}), as well as their eigenvalues (ε_1 and ε_2 with $\varepsilon_2 > \varepsilon_1$) (Doumalin and Bornert, 2000). These quantities can also be evaluated for some regions of interest, for instance, the principal average strains of the global zone E_1 and E_2, respectively. In this study, the recorded images represent a zone (256 × 221 μm^2) of the hard clay with a high resolution (4096 × 3536 pixels) (Fig.1). The physical pixel size of the images is 62.5 nm, and the size of the correlation subsets (40 × 40 pixels) for DIC analysis is 2.5 μm. According to the procedure for local strains calculation, which uses the displacements of the eight closest neighbouring positions of a given measurement position, the local gauge length is 80 × 80 pixels (i.e. 5.0 μm in real space).

It is worth noting that the accuracy of the strain determined by DIC strongly depends on the quality of ESEM images which could be degraded due to the high chamber pressure (up to 744 Pa here). Choosing optimal parameters of image acquisition (e.g. dwell time, spot size, working distance) has been made to improve the strain accuracy. Finally, the accuracy of global strain is better than 10^{-4}, while the accuracy of the local strain is in the order of 10^{-3} (Wang et al., 2014b).

3. Material and experimental procedure

Material

A natural sedimentary hard clay was studied here. The mineralogical studies show that the hard clay contains clay minerals including swelling clay mineral (e.g. smectite) and non-swelling clay minerals (e.g. illite), and inclusions (e.g. quartz, feldspar, pyrite, calcite) which are relatively rigid and non-swelling. The in situ density of the saturated material is about 1.9 g/cm^3. The permeability of the hard clay is in order of 10^{-19} m^2. The uniaxial compression strength of the saturated hard clay is about 2 MPa. The connected porosity and the pore size distribution of the material were examined using the mercury intrusion porosimetry (MIP) method. The measured connected porosity of the material is 27%.

Experimental procedure

In order to perform cyclic W-D tests, a cubic sample ($5 \times 5 \times 10$ mm^3) was machined using saw wire. For ESEM observation, one surface of the sample underwent a mechanical polishing using SiC abrasive papers and then an ion beam polishing. The observation surface is normal to the bedding plane, which is favorable to investigate the anisotropic properties of the material. Compared with the conventional mechanical polishing (Wang et al., 2013), the ion polishing after mechanical polishing can greatly enhance the surface quality. In particular, the clay particles, inter-particle pores, and secondary inclusions,are more visible (Fig.2).

The initial hydric state of the sample was unsaturated during the sample preparation process (Ewy, 2015). Accordingly, the relative humidity was firstly applied at 20%, and this was chosen as the reference state. Three W-D cycles were performed on the sample. The first W-D cycle consisted of seven hydric stages by changing the relative humidity from 20% to 50%, 80%, 90%, 98%, 80%, 20%, progressively. Both the second and third cycles consisted of three hydric stages by changing RH from 20% to 98% and 20%, successively. During each hydric stage, the target RH was attained with a constant hydric loading rate (5%RH per minute). In total, eleven hydric stages were carried out (Table 1).

4. Results and discussions

Microstructure of the hard clay

The microstructure of the natural hard clay can be revealed in the BSE image (Fig.2). The hard clay manifests an inclusion-matrix-composite microstructure. The size of these inclusions varies from several to dozens of micrometers. The clay particle exhibits a laminar shape with a typical thickness of dozens of nanometers. Pores are found in the image and can be classified into three groups: inter-particle pores, inter-aggregate pores, and space around the inclusion. The inter-particle pore is in the size of dozens of nanometers, whereas the size of inter-aggregate pore ranges from dozens of nanometers to several micrometers. The space around the inclusion owns a size comparable to the inter-aggregate pores, thus it will be classified into the inter-aggregate pore in the following. Moreover, Fig.2 clearly shows that the hard clay is globally anisotropic: inclusions, clay particles and pores are preferential to orientate vertically in the image. Based on this anisotropic texture, the bedding plane is inferred to be along the vertical axis of the image.

Macro & microscopic swelling and shrinkage of the hard clay during W-D cycles

The principal average strains (E_1 and E_2) of the hard clay subjected to three W-D cycles were quantified using DIC method. The values of the strains at different hydric stages are listed in Table 1 and are also illustrated in Fig.3. The E_2 strain progressively increases to 0.10%, 0.40%, 0.78%, and 1.10%, then decreases to 0.83% and 0.17% during the first W-D cycle. The residual strain 0.17% after this cycle implies the strain is irreversible. The irreversible swelling continues to accumulate, i.e. 0.08%=0.25%-0.17%, during the second cycle of W-D, but it tends to be stable during the third cycle (Fig.3b). The E_1 strain is much smaller than E_2, which means that the hard clay exhibits an anisotropic swelling/shrinkage during W-D. This significant anisotropic hydric deformation might be related to several factors (e.g. anisotropic swelling of clay mineral, anisotropic fabric), which will be demonstrated in the following.

The full-field principal strains (ε_2 and ε_1) during cyclic W-D of the hard clay are illustrated in Figs. 4 and 5, respectively. Figs.4a-c and Figs.5a-c correspond to the first W-D cycle, and Figs.4d-g, Figs.5d-g are the strain maps for the second and third W-D cycles. The local strains in the maps are illustrated through isolines: the grey level represents the strain magnitude. The local strain direction at 10th and 11th stage is illustrated in Fig.4h and Fig.5h through a bar: the orientation indicates the ε_2 direction. The full-field strain maps give evidence of the heterogeneous swelling of the hard clay, which becomes more and more obvious at high RH (Figs.4a-b). Correlating with the microstructure analysis presented above (Fig.2), we can find that the full-field strain field is closely related to the microstructure of the hard clay. High swelling is mainly located in the clay minerals, and the largest local strain is up to 4.0% compared with the average strain of 1.2% (Figs.4b). Besides high swelling, low strain also exists in the clay matrix. The low-swelling in these zones are mainly related to the richness of the secondary inclusions and of the non-expansive clay minerals (e.g. illite). The full-field strains at the same RH level (e.g. Figs.4b,d,f) present a very similar distribution, except the small change in magnitude. The large irreversible local strain is mainly located in the inter-aggregates in which micro-crack appears and propagates (Figs.4c,e,g).

As presented in the method section, the local strain determined corresponds to an equivalent gauge length of 5 μm, which is comparable to the size of clay aggregate containing a few dozen of clay particles with similar sub-parallel orientations. Thus, the ε_2 direction can be considered as an indicator of the clay-particle orientation. Fig.4h shows that the ε_2 directions are systematically normal to the clay-particle orientation. This agrees with the fact that the swelling of clay particles stems from separations of inter-layer and inter-particles spaces, and, thus it is privileged along the direction normal to the clay-particle orientation. Moreover, the microstructure analysis shows that the hard clay exhibits a significant anisotropic microstructure: inclusions, clay particle and different pores present a preferred orientation. This fabric anisotropy and the anisotropic swelling of clay particle contribute to the macroscopic anisotropy of the swelling of hard clay.

Figs.5a-g present the full field strains (ε_1) of the hard clay at different stages during cyclic W-D. The results show that swelling and shrinkage co-exist: the swelling is mainly located in clay minerals, and the compressive strain mainly occurs in the inter-aggregate pores. The compressive strains are related to closure of inter-aggregate pores due to the swelling of the neighboring clay particles (Fig.5a). Therefore, the swelling of clay particles and the closing of inter-aggregate pores are competitive, and the total swelling is limited. Similar to Fig.4, the ε_1 progressively increases during hydration (Figs.5a-b) and it has the nearly same value at the same RH level (e.g. Figs.5b,d,f). As discussed above, the swelling of clay particle is unidirectional, theoretically, the local strain ε_1 should be negligible relative to ε_2. But, because the microstructure is heterogeneous, some local subsets consist of both clay particles and secondary inclusions, even micro pores. The interaction between different phases (i.e. inclusions, clay particles, pores) leads to a non-negligible strain ε_1, though it is much smaller than ε_2.

Microcracking and irreversible swelling of the hard clay during W-D cycles

As shown in Figs.3b,c, the hard clay exhibits irreversible strains during the cyclic W-D. The irreversible swelling or shrinkage phenomenon during cyclic W-D has been also found in other clayey material (Alonso et al., 2005, Wang et al., 2014a). In order to further investigate the role of the microstructure on the irreversible swelling of the hard clay during cyclic W-D, two zones are chosen (zones i and ii in Fig.2), illustrated in Fig.6 and Fig.7, respectively. Fig.6 represents a zone with the size of 55 × 60 μm^2, while Fig.7 represents a zone with the size of 10 × 14 μm^2.

During the wetting stage of the first W-D cycle, microcracks progressively close due to swelling of adjacent clay particles (Fig.6b). Some microcracks close at RH=98%. During drying stage of the first W-D cycle, the microcracks re-open and propagate (Fig.6c). Microcracks become more pronounced after exposed to two W-D cycles (Fig.6e) but tend to be stable after three W-D cycles (Fig.6g). The evolution of microcracks is consistent with the measured swelling strain E_2: the irreversible strain accumulates during the first and second W-D cycles and becomes stable during the third W-D cycle (Fig.3b). This indicates the irreversibility of the global swelling is closely related to microcracking. This can be demonstrated by the full-field strain maps (Figs.4b,d,f), in which the irreversible swelling is mainly located in the space between inclusions and clay particles.

Fig.7 gives evidence of the microstructure change of the hard clay during cyclic W-D. Clay particles swell during wetting and shrink during drying. The inter-particle pores close due to swelling of clay particle and reopen due to shrinkage (Figs.7b-f). This change is irreversible during the first W-D cycle (Fig.7c) and becomes stable after two W-D cycles (Fig.7e). The inter-aggregate pore change is more significant than the inter-particle pore. The aperture of inter-aggregate pore during drying is much larger than that of the inter-particle pore (Figs.7c,e).

The microstructure analysis at two different scales shows that the irreversible is attributed by the microcracks, inter-aggregate and inter-particle pores. Relative to the reorientation and reorganization of aggregate of expansive soils during cyclic W-D, the irreversible microstructure change is mainly located in inter-aggregate pore. This means the studied hard clay has a relative stable microstructure.

5. **Summary and conclusions**

In this study, the swelling and shrinkage of a hard clay subjected to cyclic wetting and drying has been investigated combining ESEM with DIC method. Three W-D cycles have been performed on the hard clay sample in ESEM. The quantified full-field strains by DIC give evidence of significant heterogeneous deformation of the hard clay when subjected to wetting and drying. The heterogeneity of the hydric deformation is found to be closely related to the microstructure of the hard clay. Moreover, the irreversible swelling of the hard clay is found during the first W-D cycle and tends to become stable at the end of the third cycle. The microscopic analysis of the microstructure shows that the irreversible swelling is attributed to the microcracking, the change of inter-aggregate and inter-particle pores. Moreover, the anisotropic swelling and shrinkage of the hard clay is found to be related to anisotropic fabric and anisotropic swelling of clay particle.

Acknowledgements

The authors would like to thank Michel Bornert at Ecole des Ponts ParisTech (France) for the use of the images treatment program. This work is also supported by the Chinese Fundamental Research (973) Program (2015CB057906), Hubei Provincial Natural Science Foundation of China

(2018CFA012), and the Science Foundation of China University of Petroleum, Beijing (No. 2462018BJC002). These supports are gratefully acknowledged.

References

Allais, L., Bornert, M., Bretheau,T., Caldemaison, D. (1994). Experimental characterization of the local strain field in a heterogeneous elastoplastic material. *Acta Metallurgica et Materialia* **42**(11), 3865-3880.

Aksua, I. Bazilevskayab, E., Karpyna, Z.T. (2015). Swelling of clay minerals in unconsolidated porous media and its impact on permeability. *GeoResJ* **7**, 1-13.

Alonso, E.E., Romero, E., Hoffmann, C., Carcỉa-Escudero, E. (2005). Expansive bentonite-sand mixtures in cyclic controlled-suction drying and wetting. *Engineering Geology* **8**, 213-226.

Amorim, C.L., Lopes, R.T., Barroso, R.C., Queiroz, J.C., Alves, D.B., Perez, C.A., Schelin, H.R. (2007). Effect of clay–water interactions on clay swelling by X-ray diffraction. *Nuclear Instruments and Methods in Physics Research*. **580**, 768-770.

Anderson, R.L., Ratcliffe, I., Greenwell, H.C., Williams, P.A., Cliffe, S., Coveney, P.V. (2010). Clay swelling—A challenge in the oilfield. *Earth-Science Reviews* **98**, 201-216.

Bornert, M., Orteu, J. J., Roux, S. (2011). Corrélation d'images, in *Mesures de Champs et Identification en Mécanique des Solides*, edited by M. Grédiac and F. Hild, Lavoisier, Paris, chap. 6, 175-208.

Burton, G. J., Pineda, J.A., Sheng, D.C., Airey, David. (2015). Microstructural changes of an undisturbed, reconstituted and compacted high plasticity clay subjected to wetting and drying. *Engineering Geology* **193**, 363-373.

Delage, P., Menaceur, H., Tang, A.M., Talandier, J. (2014). Suction effects in deep Callovo-Oxfordian claystone. *Géotechnique Letters* **4**, 267-271.

Delville, A., Laszlo, P. (1990). The origin of the swelling of clays by water. *Langmuir* **6**, 1289-1294.

Doumalin, P., Bornert, M., 2000.Micromechanical applications of digital image correlation techniques. In *Proceedings of Interferometry in Speckle Light, Theory and Applications*. Springer, 67-74.

Eid, J., Taibi, S., Fleureau, J.M., Hattab, M. (2015). Drying cracks and shrinkage evolution of a natural silt intended for a new earth building material. Impact of reinforcement. *Construction and Building Materials* **86**, 120-132.

Ewy, R.T. (2015). Shale/claystone response to air and liquid exposure, and implications for handling, sampling and testing. *International Journal of Rock Mechanics and Mining Sciences* **80**, 388–401.

Koliji, A., Laloui, L., Cusinier, O., Vulliet, L. (2006). Suction induced effects on the fabric of a structured soil. *Transport in Porous Media* **64**(2), 261-278.

Laribi, S., Audiguier, M., Cojean, R. (2008). Assessing shrink/swell properties of two argillaceous soils from the Paris Basin: a comparison of cation exchange determination methods. *Bulletin of Engineering Geology and the Environment* **67** (3), 415-424.

Ma, R.M., Cai, C.F., Li, Z.X., Wang, J.G., Xiao, T.Q., Peng, G.Y., Yang, W. (2015). Evaluation of soil aggregate microstructure and stability under wetting and drying cycles in two Ultisols using synchrotron-based X-ray micro-computed tomography. *Soil & Tillage Research* **149**, 1-11.

Meisina, C. (2004). Swelling-shrinking properties of weathered clayey soils associated with shallow landslides. *Quarterly Journal of Engineering Geology & Hydrogeology*. **37 (2)**, 77-94.

Mitchell, J.K., Soga, K. (2005). *Fundamentals of Soil Behaviour*, *3rd edn*. John Wiley, Sons, Inc, New Jersey.

Montes-H, G., Duplay, J., Martinez, L., Mendoza, C. (2003). Swelling-shrinkage kinetics of MX80 bentonite. *Applied Clay Science* **22**, 279-293.

Osipov, V.I., Bik, N.N., Rumjantseva, N.A. (1987). Cyclic swelling of clays. *Applied Clay Science* **2**(7), 363-374.

Romero, E., Simms, P.H. (2008). Microstructure investigation in unsaturated soils: a review with special attention to contribution of mercury intrusion porosimetry and environmental scanning electron microscopy. *Geotechnical and Geological Engineering* **26**,705-728.

Sivakumar, V., Tan, W.C., Murray, E.J., Mckinley, J.D. (2006). Wetting, drying and compression characteristics of compacted clay. *Géotechnique* **56** (1), 57-62.

Sutton, M.A., Orteu, J.J., Schreier, H.W. (2009). *Image Correlation for Shape, Motion and Deformation Measurements: Basic Concepts, Theory and Applications*. Springer.

Torres-Suarez, M.C., Alarcon-Guzman, A., Moya, R.B. (2014). Effects of loading-unloading and wetting-drying cycles on geomechanical behaviors of mudrocks in the Colombian Andes. *Journal of Rock Mechanics and Geotechnical Engineering* **6**, 257-268.

Tsang, C.F., Bernier, F., Davies C. (2005). Geohydromechanical processes in the Excavation Damaged Zone in crystalline rock, rock salt, and indurated and plastic clays—in the context of radioactive waste disposal. *International Journal of Rock Mechanics and Mining Sciences* **42**, 109-125.

Viola, R., Tuller, M., Or, D., Drasdis, J. (2005). Microstructure of clay-sand mixtures at different hydration states. Proceedings of International Symposium on Advanced Experimental Unsaturated Soil Mechanics, Trento, Italy,. *In: Tarantino A, Romero E, Cui YJ (eds) Advanced experimental unsaturated soil mechanics. Taylor, Francis Group, London*, 437-442, 27-29.

Wang, L.L., Bornert, M., Chanchole, S., Héripré, E., Yang, D.S., Halphen, B., Pouya, A., Tanguy, A., Caldemaison, D. (2013). Micro-scale experimental investigation of the swelling anisotropy of the Callovo-Oxfordian argillaceous rock. *Clay Minerals* **48**, 391–402.

Wang, L.L., Bornert, M., Héripré, E., Yang, D.S., Chanchole, S. (2014a). Irreversible deformation and damage in argillaceous rocks induced by wetting/drying, *Journal of Applied Geophysics* **107**,108-118.

Wang, L.L., Bornert, M., Héripré, E., Chanchole, S., Tanguy, A. (2014b). Full-field measurements on low-strained geomaterials using environmental scanning electron microscopy and digital image correlation: improved imaging conditions, *Strain* **50**, 370-380.

Wang, L.L., Bornert, M., Héripré, E., Chanchole, S., Pouya, A., Halphen, B. (2015). Microscale insight into the influence of humidity on the mechanical behavior of mudstones. *Journal of Geophysical Research: Solid Earth* **120**(15), 3173-3186.

Wheeler, S.J., Sharma, R.S., Buisson, M.S.R. (2003). Coupling of hydraulic hysteresis and stress–strain behaviour in unsaturated soils. *Géotechnique* **53**(1), 41-54.

Yang, D.S., Bornert, M., Chanchole, S., Gharbi, H., Valli, P. (2012). Dependence on moisture content of elastic properties of argillaceous rocks investigated with optical full-field strain measurement techniques. *International Journal of Rock Mechanics and Mining Sciences* **54**, 53-62.

Yang, D.S., Chanchole, S., Valli, P. (2013). Study of the anisotropic properties of argillite under moisture and mechanical loads. *Rock Mechanics Rock Engineering* **46**(2), 247-257.

Accepted manuscript doi: 10.1680/jgeot.17.p.053

Table 1 Hydric paths of the cyclic W-D test and the corresponding principal strains of the hard clay.

Step	1st	2nd	3rd	4th	5th	6th	7th	8th	9th	10th	11th
RH (%)	20	50	80	90	98	80	20	98	20	98	20
E_1 (%)	0	0.06	0.22	0.29	0.44	0.27	-0.04	0.46	-0.01	0.36	-0.01
E_2 (%)	0	0.10	0.40	0.78	1.10	0.83	0.17	1.00	0.25	1.08	0.24

Accepted manuscript doi:
10.1680/jgeot.17.p.053

Figure 1 Schema of the zone for DIC analysis.

Figure 2 Microstructure of the natural hard clay.

Figure 3 Principal strains (E_1 and E_2) during the first W-D cycle (a); E_2 at 20% and 98% RHs during the three W-D cycles (b); E_1 at 20% and 98% RHs during the three W-D cycles (c).

Figure 4 Full-field local strain (ε_2) of the hard clay during cyclic W-D (a-g) and local strain direction (h).

Figure 5 Full-field local strain (ε_1) of the hard clay during cyclic W-D (a-g) and local strain direction (h).

Figure 6 Microcracking (zone i in Fig.2 with the size 50×60 μm^2) during cyclic W-D.

Figure 7 Evolution of pores (zone ii in Fig.2 with the size 10×14 μm^2) during cyclic W-D.

Accepted manuscript doi:
10.1680/jgeot.17.p.053

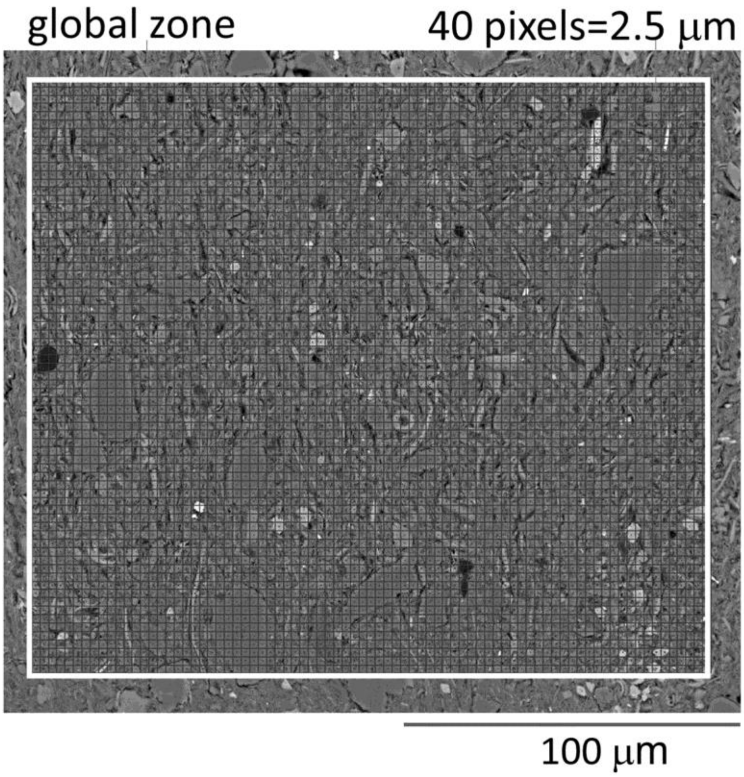

fig1n

Accepted manuscript doi:
10.1680/jgeot.17.p.053

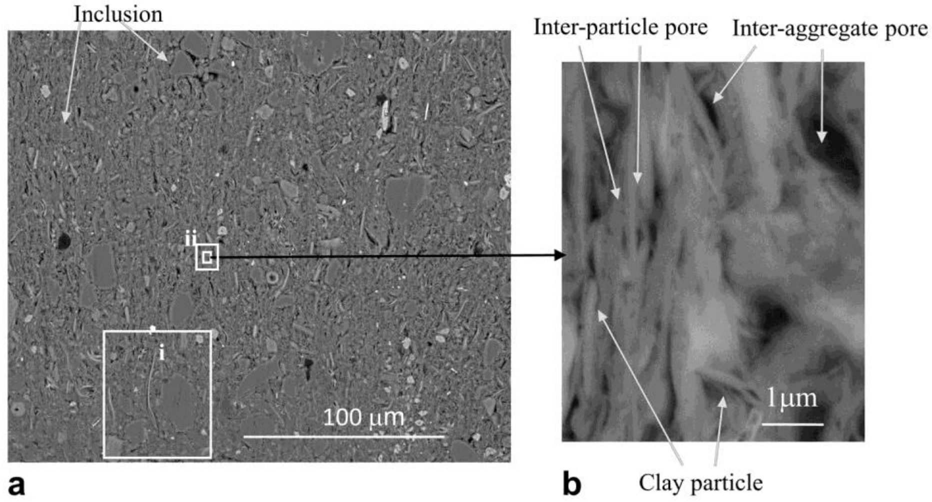

fig2n

Accepted manuscript doi:
10.1680/jgeot.17.p.053

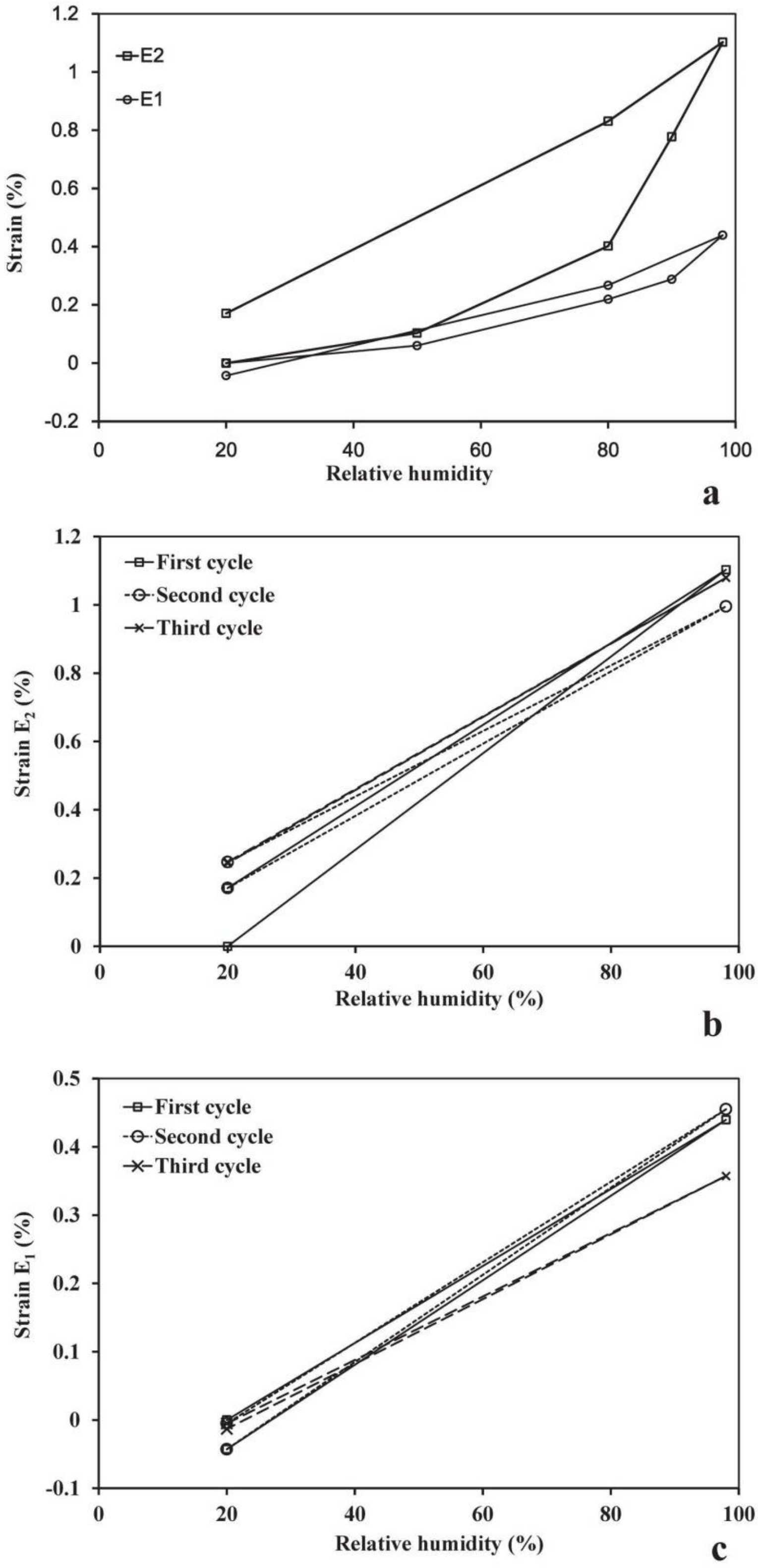

Fig.3

Accepted manuscript doi:
10.1680/jgeot.17.p.053

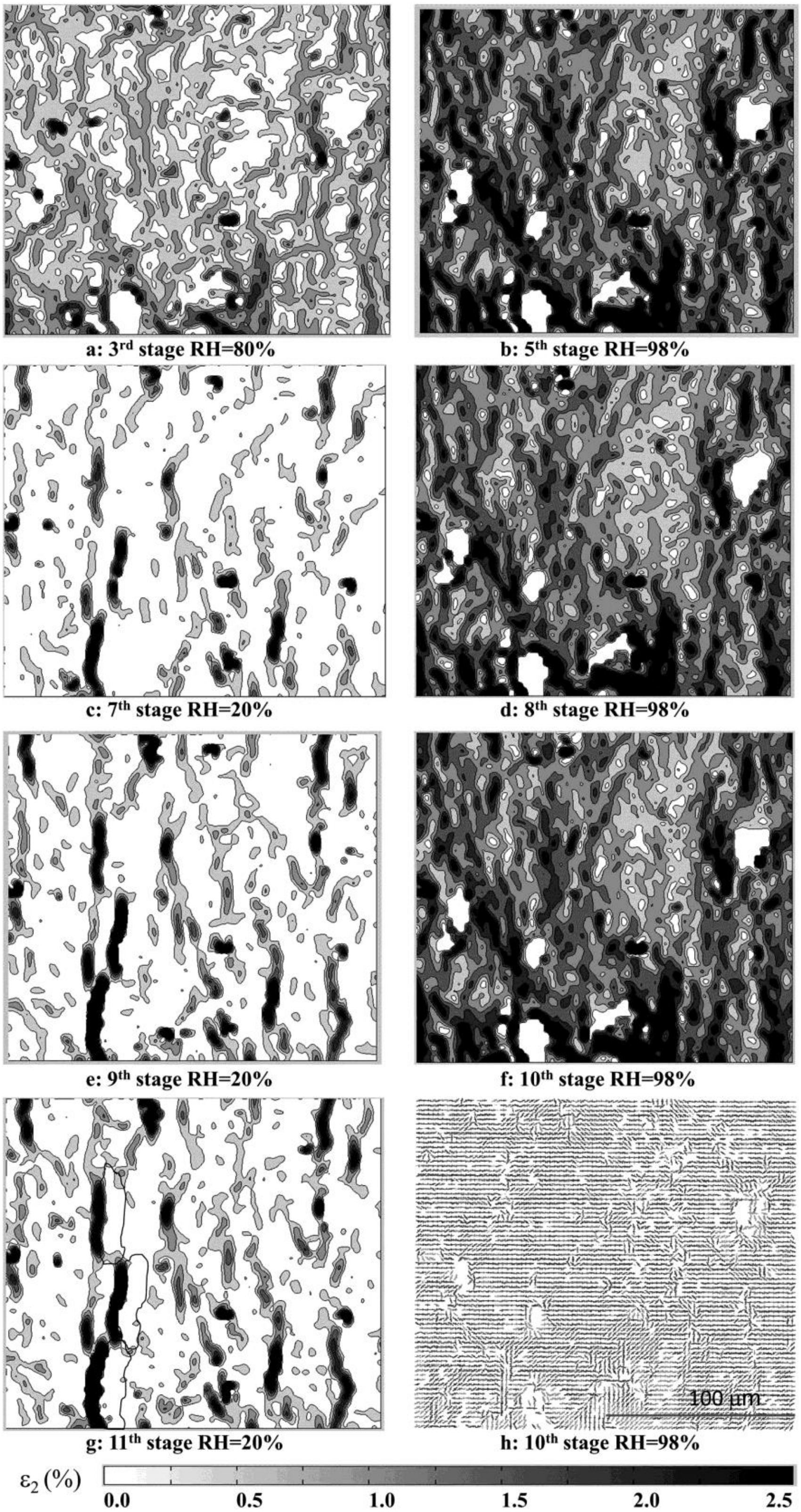

fig4n

Accepted manuscript doi:
10.1680/jgeot.17.p.053

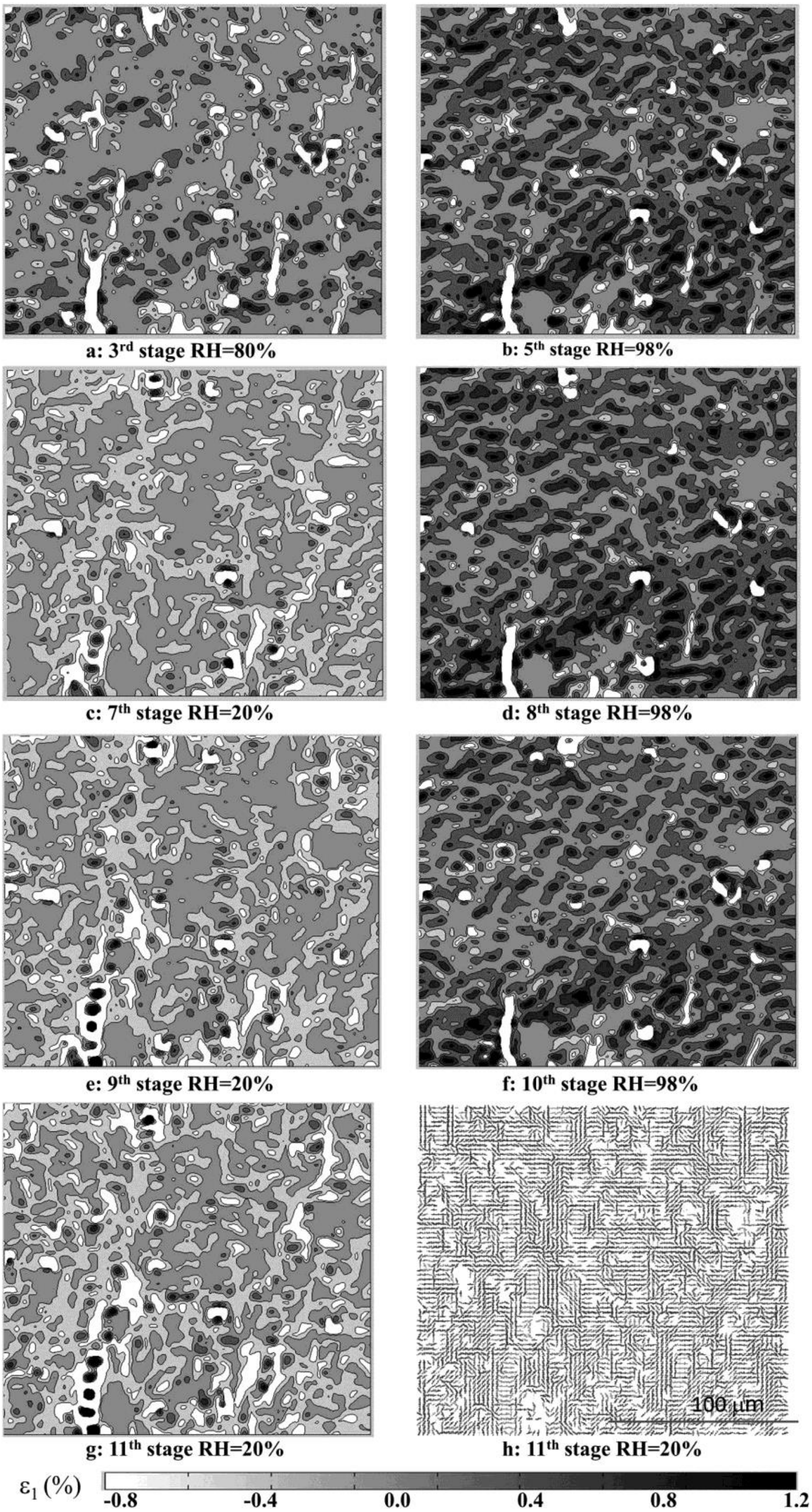

fig5n

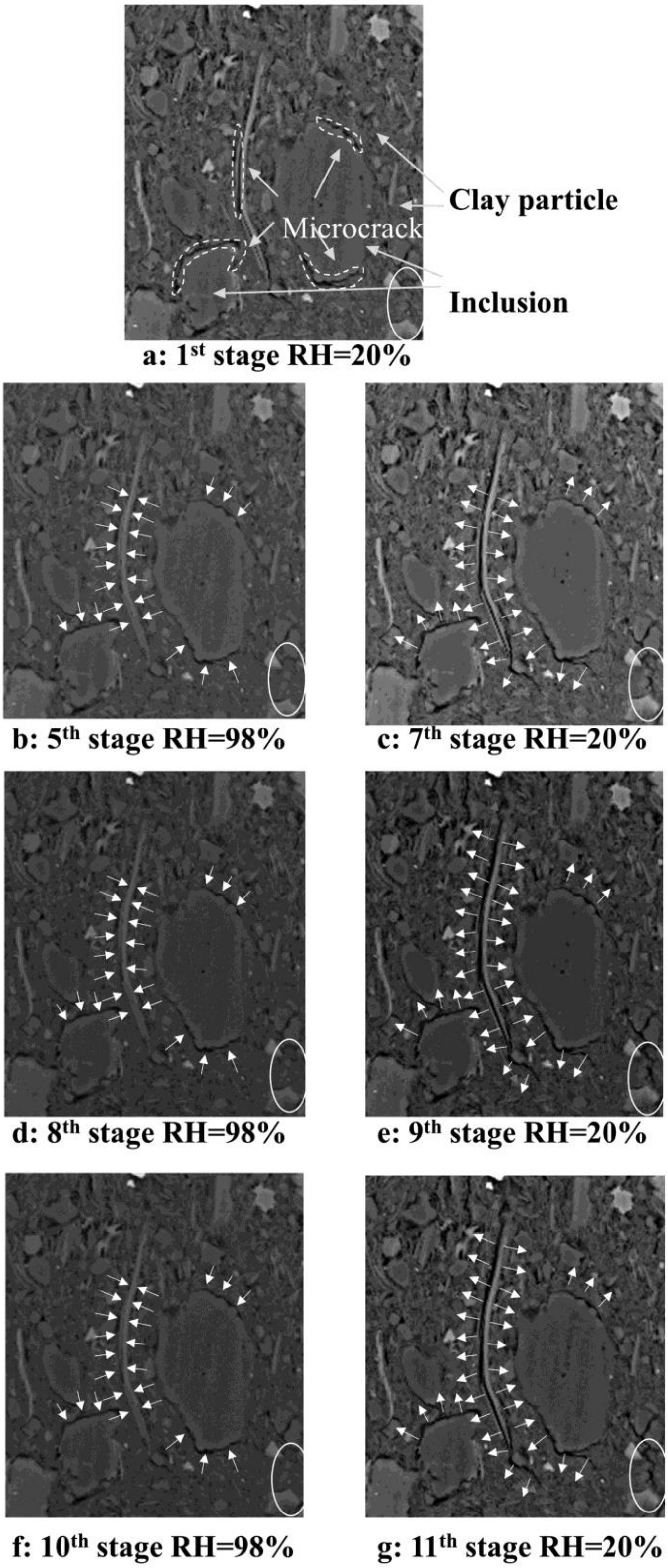
Clay particle
Microcrack
Inclusion
a: 1st stage RH=20%
b: 5th stage RH=98%
c: 7th stage RH=20%
d: 8th stage RH=98%
e: 9th stage RH=20%
f: 10th stage RH=98%
g: 11th stage RH=20%

fig6n

Accepted manuscript doi:
10.1680/jgeot.17.p.053

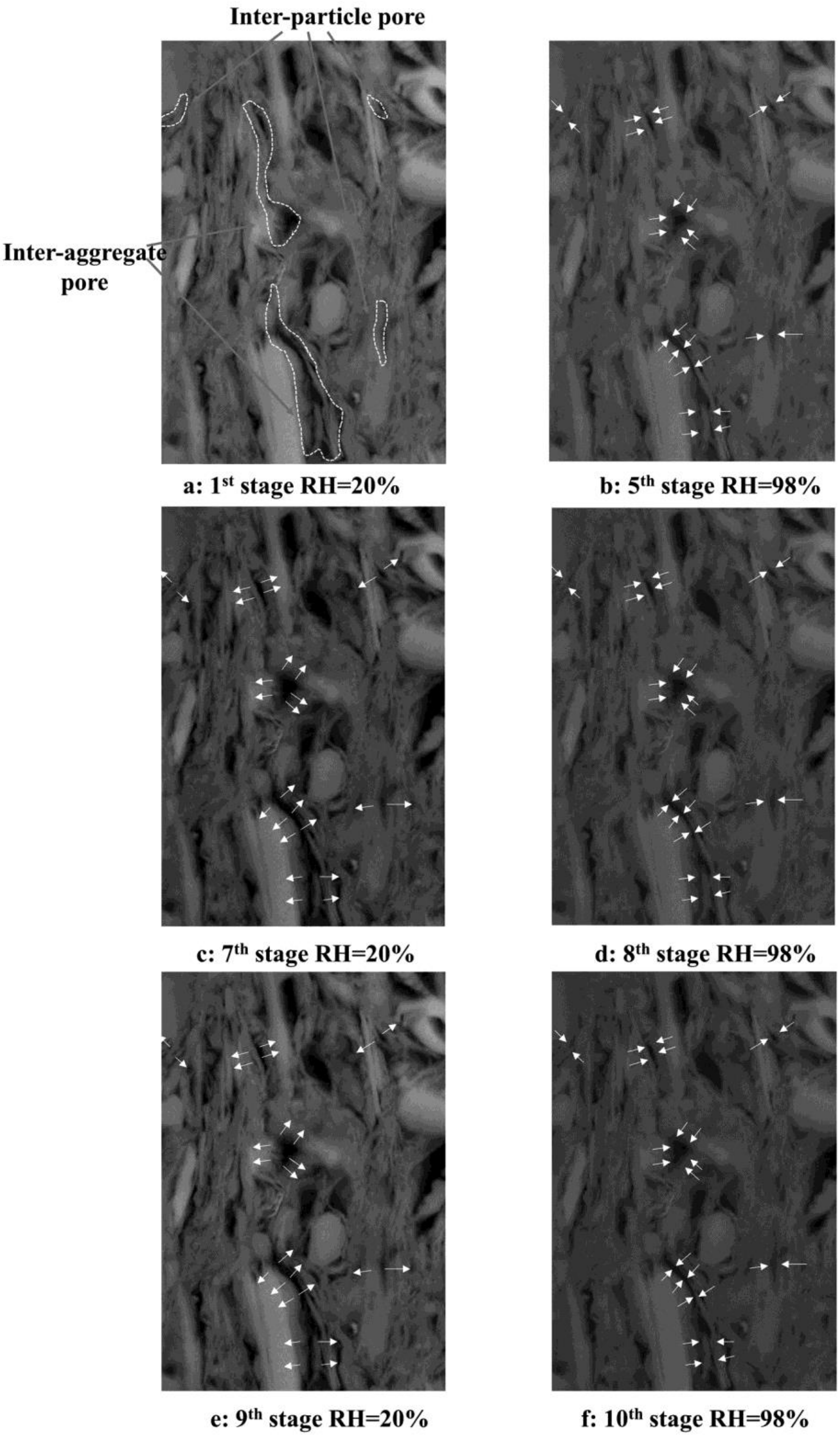

fig7n